

A Line Impedance Calculator Based on a G3 PLC Modem Platform

Giovanni Artale¹, Member, IEEE, Giuseppe Caravello², Antonio Cataliotti³, Member, IEEE, Valentina Cosentino⁴, Member, IEEE, Dario Di Cara⁵, Member, IEEE, Riccardo Fiorelli⁶, Salvatore Guaiana⁷, Nicola Panzavecchia⁸, and Giovanni Tinè⁹, Member, IEEE

Abstract—Power line communication (PLC) is one of the most today used technologies for both automatic meter reading and many other smart grid applications. In this framework, a characterization of the electrical network in the PLC frequency range is needed in terms of impedance measurement and received signal level. This can allow choosing the most suitable and less noisy frequency ranges for PLC transmission. Usually, these characterization measurements are performed with dedicated instrumentation and in the absence of mains voltage. This article wants to propose an alternative solution, which allows these kinds of measurements to be performed using electronic boards currently used as on-field applications, such as smart meters. To this aim, an innovative measurement tool is proposed, which does not need a specific characterization signal to be injected because it uses the preamble of a generic PLC transmission. Moreover, the impedance calculation is performed using an FFT analysis, which does not require high computational capabilities. These features allowed the proposed tool to be implemented using a G3-PLC transceiver, embedded in many commercial smart meters, and low-cost additional hardware. This article shows how the proposed system correctly measures the PLC impedance on CENELEC A, B, and FCC frequency ranges.

Index Terms—Communication signal, distributed measurement systems, impedance measurement of electrical network, power line communication (PLC), power system communication, power system measurements, smart grids measurements.

I. INTRODUCTION

THE evolution of today's distribution networks into smart grids involves increasing the observability of the

Manuscript received September 15, 2021; revised December 20, 2021; accepted January 8, 2022. Date of publication January 26, 2022; date of current version March 1, 2022. The research received the financial support of the European Union through the following grants: Program IEV CT Italie Tunisie 2014-2020, under Project IS_2.1_131, Solution innovantes pour l'intégration des énergies renouvelables sur le réseau électrique tunisien (SInERT), Unique Project Codes (CUP): B74119001040006 for CNR and B74118014130002 for University of Palermo; Program PO FESR Sicilia 2014-2020, Action: 1.1.5, under Project 08000PA90246, Smart grids per le isole minori (I-Sole), CUP: G99J18000540007. The Associate Editor coordinating the review process was Sara Sulis. (Corresponding author: Dario Di Cara.)

Giovanni Artale, Giuseppe Caravello, Antonio Cataliotti, and Valentina Cosentino are with the Department of Engineering, Università di Palermo, 90128 Palermo, Italy (e-mail: giovanni.artale@unipa.it; giuseppe.caravello02@unipa.it; antonio.cataliotti@unipa.it; valentina.cosentino@unipa.it).

Dario Di Cara, Salvatore Guaiana, Nicola Panzavecchia, and Giovanni Tinè are with the Institute of Marine Engineering (INM), National Research Council (CNR), 90146 Palermo, Italy (e-mail: dario.dicara@cnr.it; guaiana.salvatore@inwind.it; nicola.panzavecchia@cnr.it; giovanni.tine@cnr.it).

Riccardo Fiorelli is with STMicroelectronics S.R.L., 20864 Agrate Brianza, Italy (e-mail: riccardo.fiorelli@st.com).

Digital Object Identifier 10.1109/TIM.2022.3146629

system with the continuous and accurate measurement of various quantities, such as current, voltage, frequency, power absorbed/generated by the systems, and also power quality parameters [1]–[5]. The acquisition of such data requires metering devices located at several points in the grid and the collection of such data for centralized monitoring and control by distribution system operators (DSOs). Communication infrastructure is, therefore, essential between DSO, metering systems, and other actors involved in grid management, such as distributed generators, storage systems, and users. Among the most popular communication technologies in distribution networks, power line communication (PLC) technology has the main advantage of a reduced cost of installation because it uses the electrical network as a communication link and robustness because it is based on a wired link [6]–[11]. PLC is used worldwide on low-voltage (LV) networks for automatic meter reading, and in recent years, it has been also proposed for further applications, such as secondary substation automation, remote control of the distributed generator, and other smart grid solutions [3], [12]. However, since distribution networks were not originally designed for communication purposes, they can be affected by disturbances and attenuations, which are not easily predictable in the whole PLC frequency range. The power line behavior, in fact, is dependent not only on the electric cables' characteristics but also on the number and type of loads connected to the network. Sometimes, end-user equipment may represent a low-impedance path for the PLC signal, resulting in high signal attenuation, which may compromise the communication [13]. It is, therefore, evident how important it is to obtain information on the impedance and frequency response of the channel in order to locate the best frequency bands for signal transmission and avoid those with high levels of attenuation or noise.

PLC channel characterization is usually performed by measuring the following parameters: signal-to-noise ratio (SNR) or link quality index (LQI) [14], [15]. Another important method used for PLC channel characterization is the impedance measurement in the PLC frequency range. Electrical network impedance depends on network topology, cables, and types of connected loads. Several experiments are presented in the literature, which reports the impedance measurement versus frequency in different cases of the electrical network [16]–[18]. In some cases [19]–[21], the frequency response of the channel calculated by “channel estimation” algorithms is used to determine the real-time impedance value. Measurement

campaigns have also been carried out for different scenarios (laboratories, and urban and rural towns) [22]–[23]. The experimental results show how the access impedance has a frequency trend that depends on the network topology, the number, and the type of connected loads. Usually, the measured impedance varies between 1 and 25 Ω in urban areas, consisting of blocks of buildings, and between 30 and 70 Ω in rural areas. Furthermore, in the latter case, a noninductive behavior of the impedance is observed at measuring points far from dwellings. [23].

Another aspect to be considered is the time-varying characteristic of the impedance. In [24] and [25], it was shown how the line impedance can change with time, even within a network cycle, often showing a repetitive behavior. In this case, the measurement setup calibration is significantly time-consuming in order to obtain consistent results and highly accurate measurements [24], [25]. As an example, in [25], a measurement setup is shown which can measure down to 3 ms of impedance variability.

Another problem to be addressed in impedance measurement applications is the expected noise levels in the frequency range of interest [26]. Several investigations were carried out in the literature on the accuracy and reliability of impedance measurement techniques, taking into account the presence of noise. These included impedance measurement, frequency-domain reflectometry, and reflection coefficient measurement [27]. In this article, it is also concluded that, if transmitter, receiver, and channel noises are taken into account as possible noise sources, in order to minimize the noise in the impedance measurement technique, the shunt resistor must have a small value with respect to the real part of modem impedance.

In the abovementioned studies, usually, impedance measurement methods involve the use of network analyzers or measurement systems based on data recording and processing software. One of the main disadvantages of these measurement schemes is the need for dedicated equipment and continuous knowledge of electrical networks topology. The use of dedicated equipment and the complexity of its management results in high costs. On the other hand, the knowledge of the network topology requires a large amount of data storage to cope with the continuous reconfiguration of the network, depending on the topology of the connected loads.

In this article, a different approach is proposed based on the integration of impedance measurement techniques directly on the electronic devices, which embeds the PLC modem, such as the smart meter widely installed in distribution networks, and the use of the same PLC signal as the testing signal. In this way, two main advantages are obtained: 1) no dedicated measurement device is needed, thus significantly reducing the installation costs and 2) an impedance measurement can be theoretically obtained for each signal transmission. The use of the smart meter for PLC channel analysis was first proposed in [28], where a software tool, called *PLC Field Analyzer*, was implemented on a communication and measurement board widely used within smart meters for remote energy metering, thus significantly reducing costs and complexity of the measurement system. The ST8500 PLC modem was used as

a case study. The modem is embedded on a development board for smart grid applications, the EVALKITST8500-1. The developed tool allowed, with a simple firmware upgrade, to perform a frequency characterization of the PLC signal received on the LV network. The measurement capabilities were validated with experimental laboratory tests.

Starting from the above-described system, an upgrade of the implemented functions is proposed in this article. In detail, the software tool, presented in [28], was integrated with additional functionality to estimate the impedance pattern in the communication frequency range. The new functionality is called *line impedance calculator*, and it is based on the injection of a PLC signal superimposed on mains voltage and the measurement of voltage and current in the frequency range of interest, i.e., for CENELEC A, B, and FCC bands. The new tool's measuring technique is based on the usage of the G3-PLC signal preamble as a characterization signal over the whole frequency range. Furthermore, the impedance calculation is carried out utilizing an interpolated FFT analysis, which does not need a large amount of computer power. These characteristics enabled the suggested tool to be implemented with the aforementioned board and some low-cost extra hardware.

This article is organized as follows. Section II describes the measurement methodology used for *line impedance calculator* implementation. Section III describes the used measurement system architecture both from hardware and firmware point of view. Section IV describes the tests for measurement instrument characterization. Finally, conclusions are drawn, and future developments are envisioned.

II. MEASUREMENT METHODOLOGY

This section describes the methodology of acquisition, storage, and processing of measurement data for the impedance calculation in the frequency range of interest. The measurement methodology consists of the injection of a PLC signal and the simultaneous sampling of voltage and current values; then, the acquired signals are processed to obtain the frequency response of the network impedance shown at the connection point. An innovative feature of the adopted methodology is the use of a characterization signal intrinsically contained in the preamble of the PLC signal transmitted in the G3 protocol. The preamble of a G3 PLC signal, in fact, contains all the carriers, and thus, it can be used as a characterization signal.

In order to understand, in detail, the spectral composition of the transmitted signal, it is useful to refer to the standards that define the spectral content in the various frequency bands allowed for the PLC signal transmission. The first reference standard for the case study is ITU-T G.9901 [30], which specifies the voltage levels admissible for PLC transmission in the 9–535-kHz band, the control parameters to define the spectral content, and the parameters for controlling and reducing power spectral density. Additional information in dependence of the used communication protocols can be found in ITU-T G.9902 (G.hnem), ITU-T G.9903 (G3-PLC), and ITU-T G.9904 (PRIME). In the case of the G3-PLC protocol, ITU-T G.9903 [29] contains all specifications for both the physical layer (PHY) and the data link layer (DLL) of orthogonal frequency-division multiplexing (OFDM) modulated PLC

signals for frequencies below 500 kHz for both ac and dc electrical networks. This kind of modulation is specifically suggested by the standard because the PLC channel has a variable behavior, which strongly depends on frequency and cable characteristics but also on the number of connected loads; moreover, it is susceptible to interference, background noise, impulse noise, and group delays of up to several hundred of microseconds. OFDM modulation technique allows a very robust communication in the presence of interference, noise, and frequency selective attenuation by exploiting the whole assigned band. In addition, the use of advanced channel coding techniques ensures coexistence with other PLC technologies operating in the same frequency range. In particular, the band available in an OFDM transmission is divided into a defined number of subchannels, which can be considered as many independent PSK subcarriers modulated with orthogonal frequencies. In this way, a frequency-domain map of an OFDM symbol is obtained. The frequency components of the OFDM symbol are then transformed using an inverse fast Fourier transform (IFFT), to be represented in the time domain. In other words, the OFDM signal is generated by performing the IFFT on the complex values produced by differentially encoded phase modulation, allocated to each subcarrier. According to the specifications for G3-PLC transceivers reported in [29], the IFFT is realized on 256 points considering a sampling frequency f_s equal to 0.4 MHz for the CENELEC-A and CENELEC-B bands, and f_s equal to 1.2 MHz for the FCC band. With these values, the subcarrier frequency spacing is 1.5625 kHz (i.e., $f_s/N = 400\,000/256$) and 4.6875 kHz (i.e., $f_s/N = 1\,200\,000/256$) for CENELEC and FCC bands, respectively. As specified in [30], the IFFT is realized on 256 points considering a sampling frequency f_s equal to 0.4 MHz for the CENELEC-A and CENELEC-B bands, and f_s equal to 1.2 MHz for the FCC band. With these values, the subcarrier frequency spacing is 1.5625 kHz (i.e., $f_s/N = 400\,000/256$) and 4.6875 kHz (i.e., $f_s/N = 1\,200\,000/256$) for CENELEC and FCC bands, respectively. According to the relative bandwidths [30], the number of usable subcarriers is 36 for the CENELEC-A band (35.9375–90.625 kHz), 16 for the CENELEC-B band (98.4375–121.875 kHz), and 72 for the FCC band (154.6875–487.5 kHz).

In the PHY layer, the typical OFDM frame consists of a preamble, a control header [frame control header (FCH)], and the data section. The FCH frame consists of 13 symbols that have important control functions useful for PHY-OFDM frame demodulation. The payload duration in the time domain depends on the used modulation technique, among those available, i.e., BPSK, QPSK, 8-PSK, 16-QAM, and robust, with coherent or differential modulation scheme. In a generic frame, containing either payload data or an acknowledgment (i.e., ACK/NACK frame without payload), the preamble consists of eight identical SYNCP symbols followed by one SYNCM symbol and 1/2 SYNCM symbol. The SYNCM symbol is identical to the SYNCP symbol but shifted of π . The whole structure of a PHY-OFDM data frame is shown in Fig. 1. SYNCP and SYNCM symbols are used for

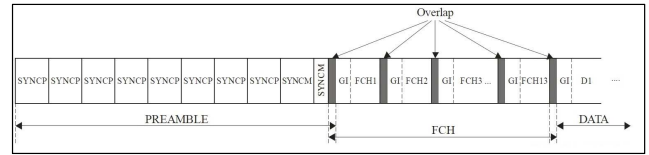


Fig. 1. PHY OFDM data frame structure.

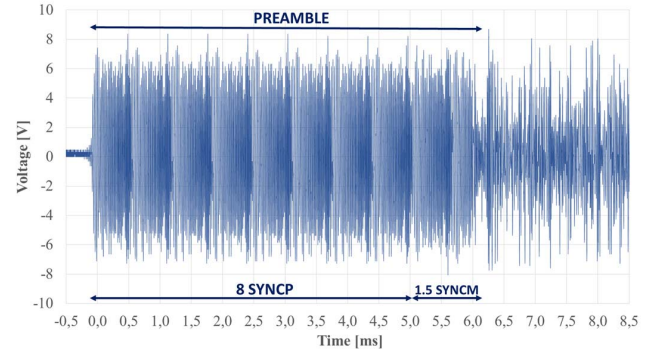


Fig. 2. OFDM preamble waveform in the CENELEC-A band.

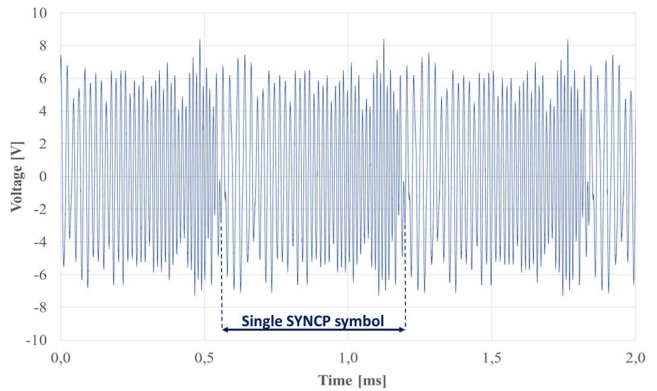


Fig. 3. Single SYNCP symbol of the OFDM preamble waveform in the CENELEC-A band.

synchronization, channel quality evaluation, and reference phase estimation, at the initial stage of communication.

The SYNCP and SYNCM symbol durations are fixed, and they depend on the used transmission band [29]. For transmissions in the CENELEC band, the duration of the SYNCP/SYNCM symbol is 640 μ s, while, for transmissions in the FCC band, it is 213 μ s.

To confirm this, Figs. 2 and 3 show the time trends of the preamble and of a single SYNCP measured in the CENELEC-A band. The measurement was performed on the signal transmitted by an EVLKITST8500-1 board configured for G3-PLC communications. The signal was acquired with a Rohde & Schwarz RTO 1044 oscilloscope with frequency samples of 200 MSa/s.

Since the single SYNCP/SYNCM symbol does not contain any specific information, the associated OFDM signal is obtained by applying the IFFT to the complex-valued

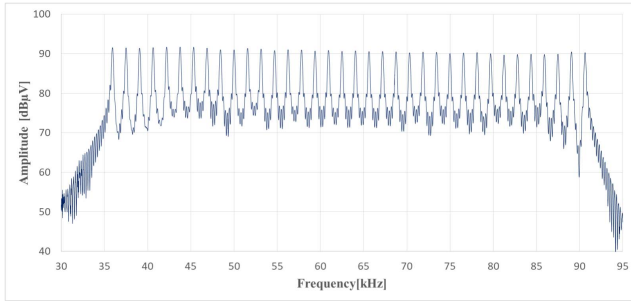


Fig. 4. Spectrum of the SYNCP symbol in the CENELEC-A band.

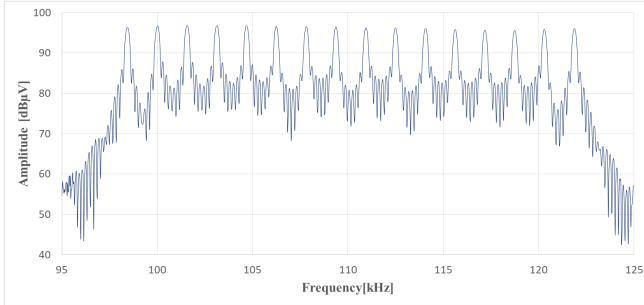


Fig. 5. Spectrum of the SYNCP symbol in the CENELEC-B band.

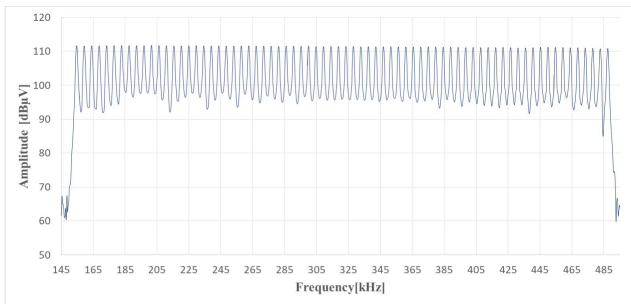


Fig. 6. Spectrum of the SYNCP symbol in the FCC band.

points corresponding to all subcarriers in the used transmission band. This means that, in the frequency domain, the spectrum content of the single SYNCP/SYNM symbol consists of a number of lines corresponding to that of all the used subcarriers. In particular, the CENELEC-A band spectrum contains 36 subcarriers spaced on 1.5625 kHz, the CENELEC-B spectrum contains 16 subcarriers spaced on 1.5625 kHz, and the FCC spectrum contains 72 subcarriers spaced on 4.6875 kHz. To confirm this, Figs. 4–6 show the preamble spectrum of an SYNCP symbol for CENELEC A, B, and FCC bands, respectively. The measured spectrum confirms the presence of all subcarriers and, therefore, the possibility of using this signal for channel characterization.

The analysis carried out so far shows the characteristics of the OFDM signal preamble on which the proposed impedance measurement methodology is based. In detail, the impedance value is determined by measuring voltage and current at each subcarrier. In this way, the impedance frequency trend can be obtained for the whole frequency range with a resolution

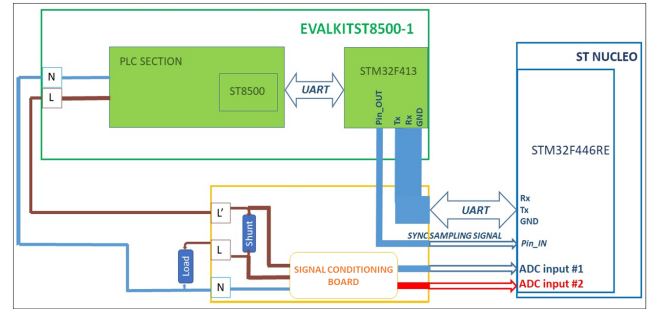


Fig. 7. Connection diagram of the boards of the line impedance calculator measurement system.

equal to the frequency spacing between the subcarriers. The impedance trend, thus, has a resolution of 1.5625 kHz for the CENELEC bands and 4.6875 kHz for the FCC band. Since the subcarriers are all contained on a single SYNCP symbol, the observation window is equal to $640 \mu\text{s}$ for the CENELEC band and $213 \mu\text{s}$ for the FCC band. To choose the sampling frequency, the higher order carrier should be considered. For the CENELEC-A band, the last subcarrier is located at 90.625 kHz; for the CENELEC-B band, it is located at 121.875 kHz; and for the FCC band, it is located at 487.5 kHz [29]. This means that the minimum sampling frequency must be greater than 181.25, 243.75, and 975 kHz, respectively. To keep the computational cost low and to reduce the calculation time, the complex fast Fourier transform (CFFT) algorithm is applied to the acquired samples [31]. The use of this algorithm allows the calculation of real and imaginary parts of each spectrum component. In this way, it is possible to determine both the amplitude and phase of each spectral component. The FFT computation within impedance calculation time was experimentally measured by the procedure adopted in [31]: the overall time needed is 9.4 ms. This result shows that the time variance of the impedance value can be recorded approximately in half a period of the mains voltage. The accuracy of the proposed system is lower than, for example, an *ad hoc* system, such as the one developed in [25], but certainly acceptable from the point of view of the hardware specifications of the low-cost commercial evaluation boards used.

III. MEASUREMENT SYSTEM: THE LINE IMPEDANCE CALCULATOR

In order to implement the proposed measurement methodology, the scheme shown in Fig. 7 has been implemented. It foresees the use of an EVALKITST8500-1 board for PLC signal injection, an ST NUCLEOF446RE for impedance acquisition and calculation, and a signal conditioning board. In a possible future evolution, the three boards could be integrated into a single board. The properties and functions of the various boards are below described in detail.

The EVALKITST8500-1 is a modular evaluation board consisting of a motherboard and a PLC transceiver. The motherboard is based on the STM32F413 microcontroller with the ARM Cortex M4 processor up to 100 MHz, the FPU unit,

and several communication peripherals (16 DMA channels, ten USARTs, five I²C's, five SPIs, one SDIO Interface, and one USB 2.0 full speed). The transceiver is the ST8500, which allows PLC communications up to 500 kHz with different protocol standards.

The ST NUCLEO F446RE is an evaluation board based on a high-performance microcontroller. The microcontroller is the STM32F446RE based on an ARM Cortex M4, with a frequency up to 180 MHz, FPU unit, DSP instructions, 512 kB of flash memory, 128 KB of SRAM memory, 16 DMA channels, and 12-bit resolution 2.4-MS/S ADCs up to 24 channels.

The combined use of the two boards makes it possible to implement the *line impedance calculator*. This functionality has been added to the software tool developed for the EVALKITST8500-1 in [28]. More in detail, the *PLC Field Analyzer* tool, developed in [28] for characterizing the quality of the received PLC signal, was included on an “RX METRIC” tab in the graphical user interface (GUI) called Smart Grid LabTool from ST Microelectronics. The firmware developed and implemented for the PLC Field Analyzer has been modified, to add the new functionality of the line impedance calculator. Moreover, this new functionality was also integrated into the same GUI on a “TX METRIC” tab.

In detail, the following features have been added to the firmware:

- 1) handling of the request from the Smart Grid LabTool for the calculation of the impedance frequency trend;
- 2) automatic configuration of a G3-PLC transmission in one of the three bands;
- 3) communication with STNUCLEO F446RE to define processing parameters and manage the reception of processed impedance values;
- 4) forwarding impedance values to the Smart Grid LabTool panel for displaying the processed results.

On the other side, on the ST NUCLEO F446RE board microcontroller, firmware has been developed and implemented with the following functionalities:

- 1) automatic configuration of the ADC block for sampling the voltage signal transmitted by the EVALKITST8500 and the associated current signal, based on the selected bandwidth;
- 2) running the linear-CFFT algorithm on acquired voltage and current samples;
- 3) processing of results obtained from CFFT calculation;
- 4) forwarding of magnitude and phase of impedance values for the selected band.

To sample a single SYNCP symbol of the preamble, the observation window was synchronized with the G3-PLC signal, by using a synchronization signal generated by the EVALKITST8500-1 board. Voltage and current signals are simultaneously sampled by using two different ADCs of the STM32F446RE. More in detail, the observation window has a fixed value, equal to the single SYNCP symbol duration, i.e., $T_w = 640 \mu\text{s}$ in the CENELEC bands and $T_w = 213 \mu\text{s}$ in the FCC band. The sampling frequency choice is based on the last OFDM signal subcarrier. On the other hand, it should be

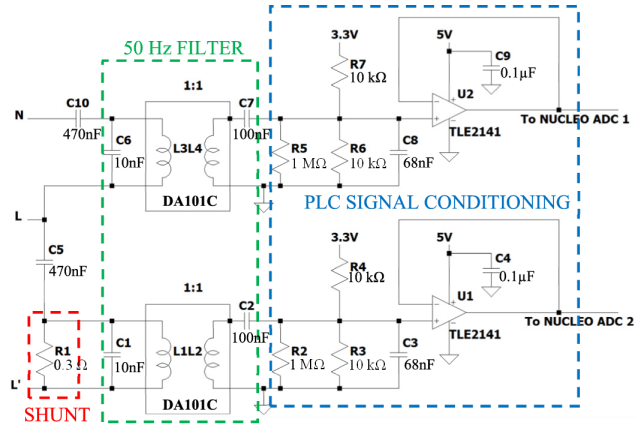


Fig. 8. Signal conditioning board for the connections between EVALKITST8500-1 and ST NUCLEO F446RE.

selected among the available values of STM32F446RE ADCs, i.e., as a submultiple, among the selectable ones, of the ADC internal clock. The chosen sampling frequencies are 1.33 and 6.06 MHz for CENELEC and FCC bands, respectively. In this way, 852 samples (i.e., $N = T_w * f_s = 640 * 1.33$) are acquired for the SYNCP symbol of the preamble in the CENELEC band and 1290 samples (i.e., $N = T_w * f_s = 213 * 6.06$) for the SYNCP symbol in the FCC band. The digitized values transfer is performed via direct memory access (DMA) of the STM32F446RE to reduce the latency.

To adapt the ADC voltage input to voltage and current signals, the signal conditioning board shown in Fig. 8 was designed. It performs the following functions:

- 1) filtering the PLC signal from the ac component at 50 Hz;
- 2) providing a voltage signal proportional to the current signal in the whole frequency range of interest (30–500 kHz);
- 3) adapting the signal values to the ADC input.

The different parts of the circuit are highlighted in Fig. 8 to show the correspondent functionalities. Based on the considerations of [27], to minimize the noise in the impedance measurement technique, a shunt resistor has to be tuned to a small value. On this basis, the current to voltage transduction is performed by means of a 0.3- Ω shunt (with an accuracy of 1%), connected in series with the load.

The flow diagram, as shown in Fig. 9, summarizes the sequence of operations carried out by the line impedance calculator and is described as follows.

- 1) A request is sent from the “TX_METRICS” panel of the Smart Grid LabTool (as shown in Fig. 10) to the EVALKITST8500-1, via USB, choosing one of the three transmission bands.
- 2) The EVALKITST8500-1 sends via UART a configuration message to the NUCLEO board to choose the proper sampling frequency based on the selected transmission band.
- 3) A *READY* status acknowledge reply is sent when the ADC configurations are complete.
- 4) The EVALKITST8500 –1 starts the PLC signal transmission and sends a trigger to the ADCs in the

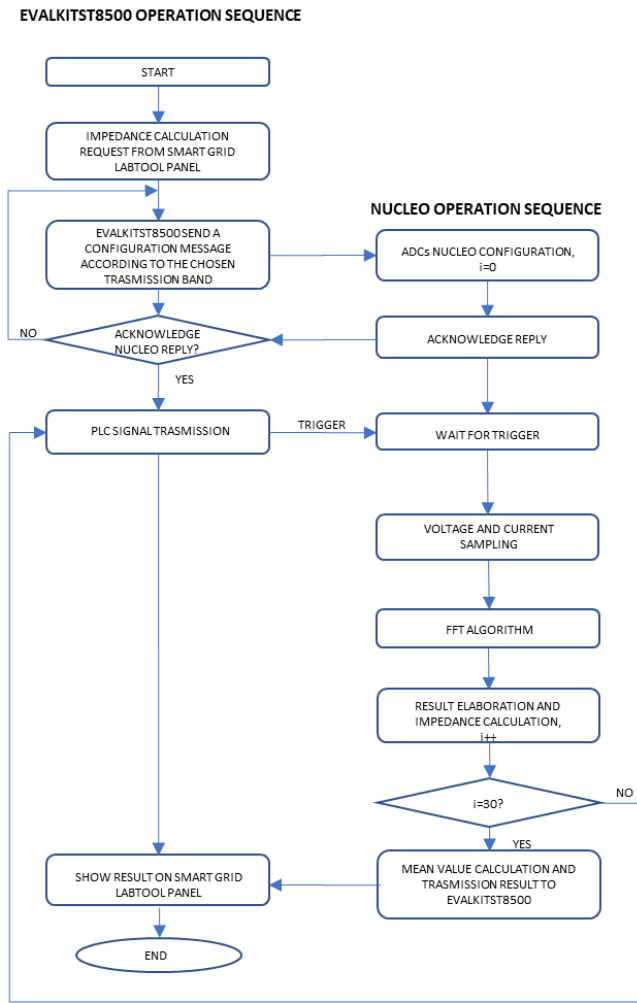


Fig. 9. Flowchart of operation sequences performed by EVALKITST8500-1 and NUCLEO boards for impedance calculation.

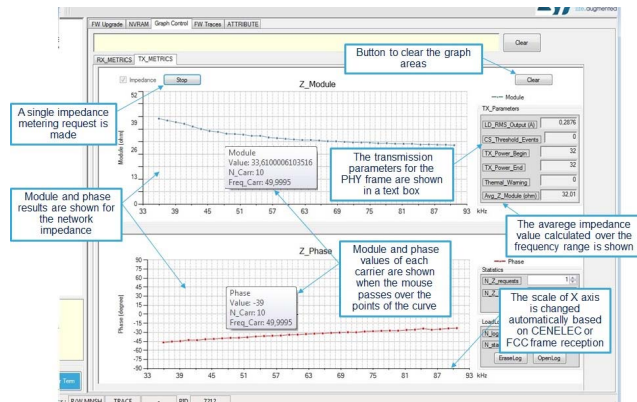


Fig. 10. Line impedance calculator front panel on the Smart Grid LabTool.

STM32F446RE of the NUCLEO board via a digital output to start the voltage and current sampling (*sync sampling signal*).

- 5) When the acquisition is completed, the STM32F446RE of the NUCLEO board performs the impedance calculation by performing the spectral analysis (CFFT algorithm).

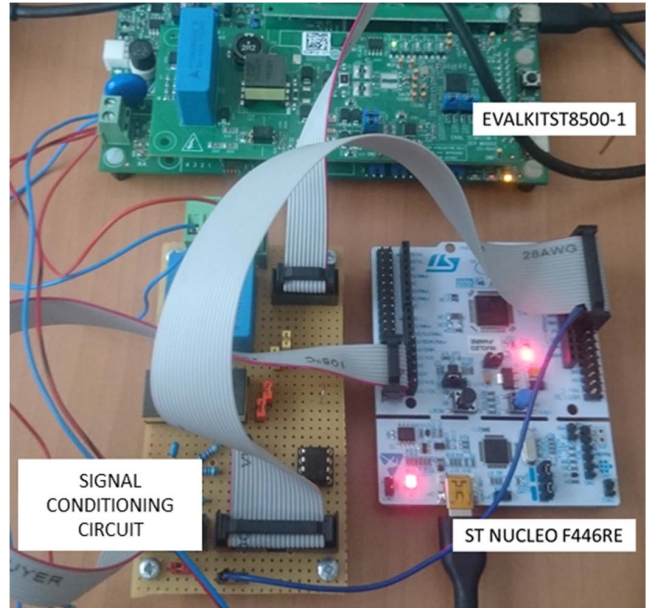


Fig. 11. Measurement system of the line impedance calculator.

- 6) To reduce the noise, which affects voltage and current signals, the above-described *PLC signal transmission–sampling–CFFT calculation* sequence is performed 30 times. The mean value is then calculated for the 30 measurements performed at each carrier frequency.
- 7) The NUCLEO board transfers the impedance results to the EVALKITST8500-1 and then to the Smart Grid LabTool, which shows the results on the “TX_METRIC” panel, as shown in Fig. 10.

IV. EXPERIMENTAL TESTS AND RESULTS

The *line impedance calculator* was tested using the measurement system shown in Fig. 11, which consists of three boards: the EVALKITST8500-1, the ST NUCLEO F446RE, and the signal conditioning circuit. The measuring system was tested by connecting loads of known values.

In detail, resistive–inductive and resistive–capacitive loads were considered. The values of the loads were selected in order to have a typical frequency trend that can occur in a power line.

The impedance values were also measured with a Keysight ENA E5080A vector network analyzer (VNA) [32]. The VNA has been set with an resolution bandwidth (RBW) equal to 300 Hz. A full one-port manual calibration was performed before each series of measurements by using a Keysight 85032F calibration kit [33]. The features of the standard connectors of the calibration kit are the following: open-circuit standard with a phase uncertainty smaller than 1.0° ; short-circuit standard with a phase uncertainty smaller than 1.0° ; and match-circuit standard with a return loss higher than 48 dB. All these parameters are defined in the frequency range of 9 kHz–10 MHz. After system error correction, the accuracies of reflection measurements are 0.1 dB and 1° in the frequency range of the considered band.

Several tests with different impedance values were carried out. All results are shown in Table I. Some of those tests are given below as examples for the CENELEC and FCC bands.

TABLE I
EXPERIMENTAL RESULTS

Frequency band	Load Impedance Value	Magnitude Mean Error (Ω)	Phase Mean Error (deg)
CENELEC-A	R = 3.3 Ω	0.24	0.96
CENELEC-A	R = 4.7 Ω	0.19	1.57
CENELEC-A	R = 10 Ω	0.29	1.34
CENELEC-A	R = 15 Ω	0.36	1.01
CENELEC-A	RL series R = 3.3 Ω , L = 10 μ H	0.33	0.37
CENELEC-A	RL series R = 10 Ω , L = 33 μ H	0.68	1.57
CENELEC-A	RL series R = 24 Ω , L = 100 μ H	2.57	0.54
CENELEC-A	RC series R = 3.3 Ω , C = 820 nF	0.2	1.44
CENELEC-A	RC series R = 10 Ω , C = 330 nF	0.6	0.37
CENELEC-A	RC series R = 24 Ω , C = 150 nF	2.15	3.46
CENELEC-B	R = 3.3 Ω	0.19	1.29
CENELEC-B	R = 4.7 Ω	0.12	2.28
CENELEC-B	R = 10 Ω	0.20	1.79
CENELEC-B	R = 15 Ω	0.26	1.32
CENELEC-B	RL series R = 24 Ω , L = 100 μ H	0.45	1.79
CENELEC-B	RC series R = 24 Ω , C = 15 nF	1.9	0.39
FCC	R = 3.3 Ω	0.23	3.25
FCC	R = 4.7 Ω	0.27	1.29
FCC	R = 10 Ω	0.16	2.25
FCC	R = 15 Ω	0.26	3.03
FCC	RL series R = 24 Ω , L = 10 μ H	0.99	1.24
FCC	RC series R = 24 Ω , C = 47 nF	0.77	1.21

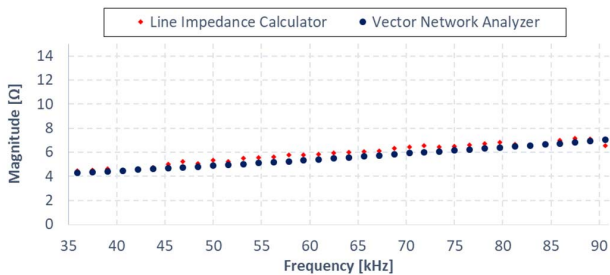


Fig. 12. Magnitude comparison between measured values by reference instrument and line impedance calculator in the case of a resistive-inductive load of 3.3 Ω and 10 μ H. Mean error = 0.79 Ω .

The first test performed in the CENELEC-A band was about a resistive-inductive load consisting of a 3.3- Ω resistor connected in series to a 10- μ H inductor. Figs. 12 and 13 show

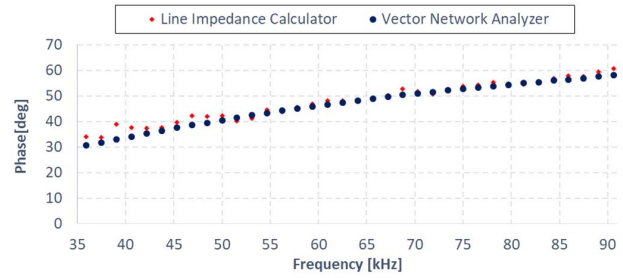


Fig. 13. Phase comparison between measured values by reference instrument and line impedance calculator in the case of a resistive-inductive load of 3.3 Ω and 10 μ H. Mean error = 2.03°.

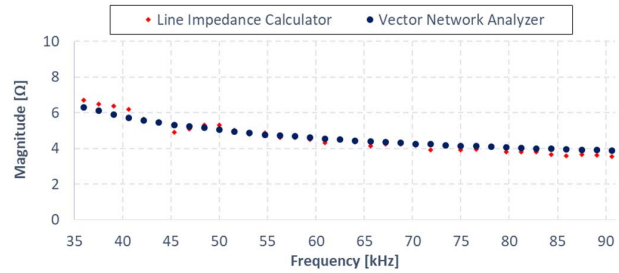


Fig. 14. Magnitude comparison between measured values by reference instrument and line impedance calculator in the case of a resistive-capacitive load of 3.3 Ω and 820 nF. Mean error = 0.20 Ω .

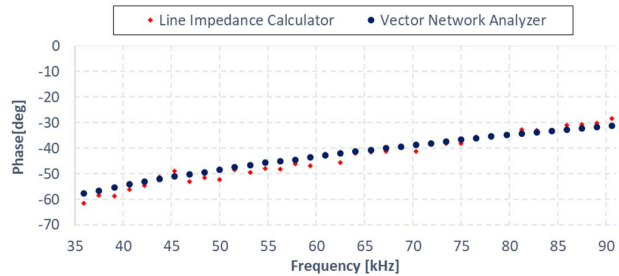


Fig. 15. Phase comparison between measured values by reference instrument and line impedance calculator in the case of a resistive-capacitive load of 3.3 Ω and 820 nF. Mean error = 1.44°.

the magnitude and phase results of the impedance measured with the proposed system (i.e., the *line impedance calculator*) in comparison with that measured by the reference instrument (the VNA). As it can be seen, the impedance measured by the proposed system has the same frequency trend as that measured by VNA. Moreover, mean errors of 0.79 Ω and 2.03 °C were observed over the entire frequency range in amplitude and phase measurements, respectively. These errors are compatible with the VNA accuracy specifications, and they can be considered acceptable for a diagnostic tool.

The second test in the CENELEC-A band was performed connecting a resistive-capacitive load consisting of a 3.3- Ω resistor connected in series to an 820-nF capacitor. Figs. 14 and 15 show the measured results with the two measurements systems. As it can be seen also in this case, the measured frequency trends are the same as those obtained with the VNA, and the measurements are compatible with

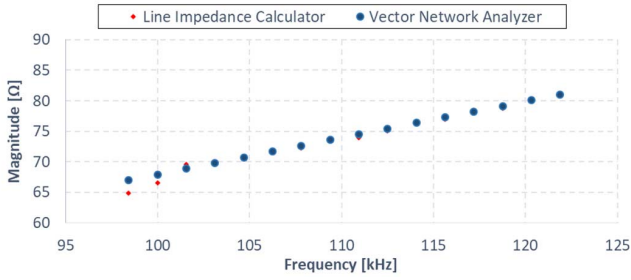


Fig. 16. Magnitude comparison between measured values by reference instrument and line impedance calculator in the case of a resistive-inductive load of $24\ \Omega$ and $100\ \mu\text{H}$. Mean error = $0.45\ \Omega$.

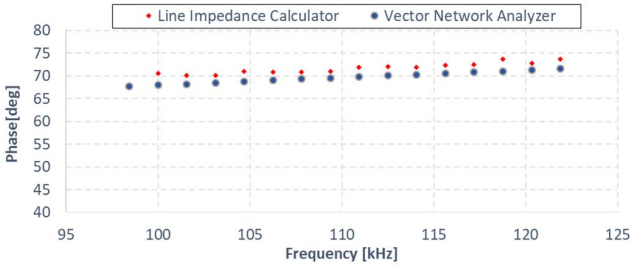


Fig. 17. Phase comparison between measured values by reference instrument and line impedance calculator in the case of a resistive-inductive load of $24\ \Omega$ and $100\ \mu\text{H}$. Mean error = 1.79° .

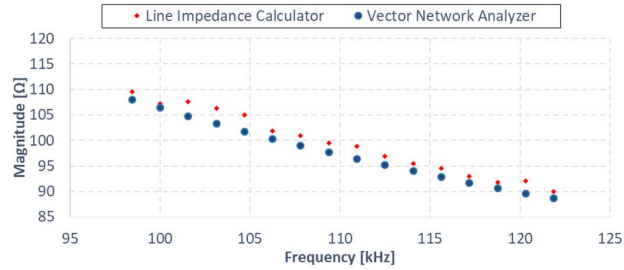


Fig. 18. Magnitude comparison between measured values by reference instrument and line impedance calculator in the case of a resistive-capacitive load of $24\ \Omega$ and $15\ \text{nF}$. Calculator. Mean error = $1.90\ \Omega$.

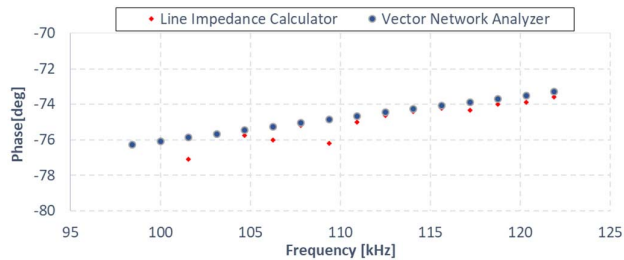


Fig. 19. Phase comparison between measured values by reference instrument and line impedance calculator in the case of a resistive-capacitive load of $24\ \Omega$ and $15\ \text{nF}$. Mean error = 0.39° .

a mean error of $0.20\ \Omega$ and 1.44° in amplitude and phase, respectively.

Similar tests were performed also in the CENELEC-B band. A resistive-inductive load was used consisting of a $24\text{-}\Omega$ resistor connected in series to a $100\text{-}\mu\text{H}$ inductor. The results

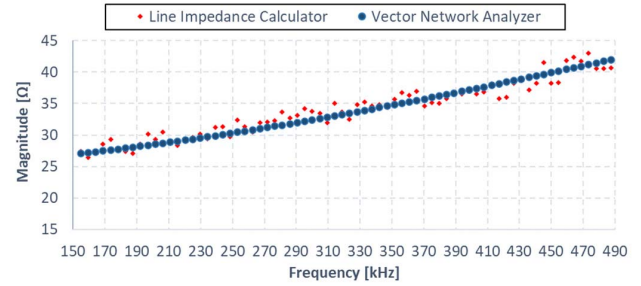


Fig. 20. Magnitude comparison between measured values by reference instrument and line impedance calculator in the case of a resistive-inductive load of $24\ \Omega$ and $10\ \mu\text{H}$. Mean error = $0.99\ \Omega$.

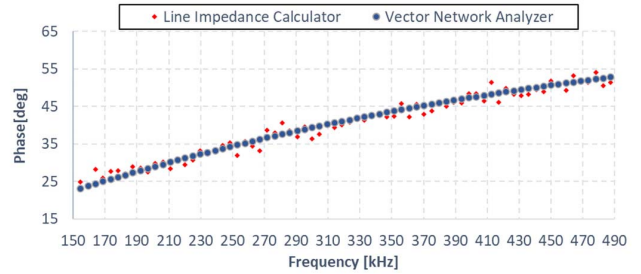


Fig. 21. Phase comparison between measured values by reference instrument and line impedance calculator in the case of a resistive-inductive load of $24\ \Omega$ and $10\ \mu\text{H}$. Mean error = 1.24° .

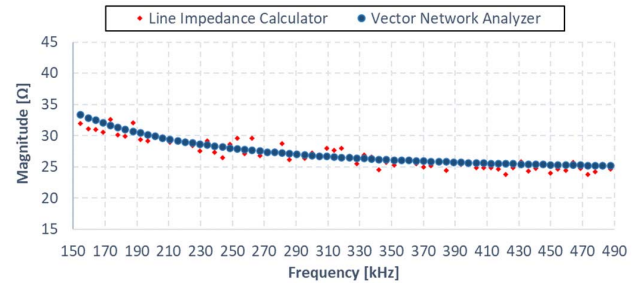


Fig. 22. Magnitude comparison between measured values by reference instrument and line impedance calculator in the case of a resistive-capacitive load of $24\ \Omega$ and $47\ \text{nF}$. Mean error = $0.77\ \Omega$.

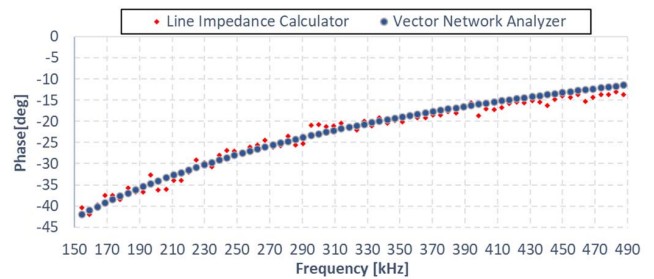


Fig. 23. Phase comparison between measured values by reference instrument and line impedance calculator in the case of a resistive-capacitive load of $24\ \Omega$ and $47\ \text{nF}$. Mean error = 1.21° .

are shown in Figs. 16 and 17. Also, in this case, frequency trends are the same, and measurements are compatible, with mean errors of $0.45\ \Omega$ and 1.79° , respectively. Similar results

were also obtained with a resistive–capacitive load, consisting of a 24- Ω resistor connected in series to a 15-nF capacitor. The results are shown in Figs. 18 and 19 for amplitude and phase, respectively.

Finally, further tests were performed also for the FCC band, with a resistive–inductive load consisting of a 24- Ω resistor connected in series with a 10- μ H inductor. The results are shown in Figs. 20 and 21 for amplitude and phase, respectively. In this case, the frequency trend is again very similar to that of the VNA, with mean errors of 0.99 Ω and 1.24°. Similar results were also obtained in the case of a resistive–capacitive load with a 24- Ω resistor connected in series to a 47-nF capacitor. The results are shown in Figs. 22 and 23 for amplitude and phase, respectively.

V. CONCLUSION

In this article, a new measurement system is proposed for power line characterization in the PLC frequency range. The new system is based on the use of smart meter electronic boards and low-cost additional hardware for characterization and measurement, thus avoiding the use of dedicated equipment and complex data processing software and recording hardware.

In fact, a new firmware was developed for both the received signal quality analysis (*PLC Field Analyzer* tool) and the power line impedance measurement (*line impedance calculator* tool). The first tool, presented in [28], allows measuring the received signal and noise levels and calculating the SNR for each carrier of the modulated signal. The second one, presented in detail in this article, is able to estimate the impedance trend of the communication channel by using the same PLC signal for characterization. The developed measurement tools were validated through several experimental tests using loads of known values and comparing the measured values with those obtained using a reference instrument. A small difference was observed between these measurements, thus validating the measurement capability of the developed instrument. Unlike *ad hoc* systems in which measurements can be performed on a sample basis, the proposed system, being embedded in a single board, is able to make a time-varying measurement for each signal transmission. With these two tools embedded, e.g., in a smart meter, the PLC channel can be fully characterized directly by the application, greatly reducing the cost and complexity of the measurement system. The results obtained show that the characteristics of the diagnostic tool would be optimal for the characterization of the communication channel with connected points located at great distances, e.g., rural networks, where the value of the impedance is very high and can also have a noninductive behavior. The embedded diagnostic tool could be also used to locate possible frequency bands with a higher level of attenuation or noise and choose the proper frequency bands for optimal transmission. The described procedures can be executed as a diagnostic tool for an operator who wants to investigate the network behavior via the Smart Grid LabTool. However, in future work, these procedures could be performed also automatically at each signal transmission; the obtained impedance values could

be then stored for post diagnosis, or they can be used to periodically adapt the transmission frequencies to the channel behavior.

ACKNOWLEDGMENT

The authors wish to thank the engineers of the STMicroelectronics Laboratory, Rennes, France, for their scientific support. This article’s content is solely the responsibility of the authors, and it does not necessarily reflect the point of view of the European Union or that of the Program Managing Authority.

REFERENCES

- [1] M. L. Tuballa and M. L. Abundo, “A review of the development of smart grid technologies,” *Renew. Sustain. Energy Rev.*, vol. 59, pp. 710–725, Jun. 2016.
- [2] G. D’Avanzo, A. Delle Femine, D. Gallo, C. Landi, and M. Luiso, “Impact of inductive current transformers on synchrophasor measurement in presence of modulations,” *Measurement*, vol. 155, Apr. 2020, Art. no. 107535.
- [3] E. Kabalci and Y. Kabalci, “A measurement and power line communication system design for renewable smart grids,” *Meas. Sci. Rev.*, vol. 13, no. 5, pp. 248–252, Oct. 2013.
- [4] A. Cataliotti, V. Cosentino, D. Di Cara, A. Lipari, S. Nuccio, and C. Spataro, “A PC-based wattmeter for accurate measurements in sinusoidal and distorted conditions: Setup and experimental characterization,” *IEEE Trans. Instrum. Meas.*, vol. 61, no. 5, pp. 1426–1434, May 2012.
- [5] G. Crotti, D. Giordano, G. D’Avanzo, P. S. Letizia, and M. Luiso, “A new industry-oriented technique for the wideband characterization of voltage transformers,” *Measurement*, vol. 182, Sep. 2021, Art. no. 109674.
- [6] S. K. Rönnerberg *et al.*, “On waveform distortion in the frequency range of 2 kHz–150 kHz—Review and research challenges,” *Electr. Power Syst. Res.*, vol. 150, pp. 1–10, Sep. 2017.
- [7] G. Artale *et al.*, “A new PLC-based smart metering architecture for medium/low voltage grids: Feasibility and experimental characterization,” *Measurement*, vol. 129, pp. 479–488, Dec. 2018.
- [8] E. Kabalci, Y. Kabalci, and I. Develi, “Modelling and analysis of a power line communication system with QPSK modem for renewable smart grids,” *Int. J. Electr. Power Energy Syst.*, vol. 34, no. 1, pp. 19–28, Jan. 2012.
- [9] A. Cataliotti *et al.*, “A prototypal architecture of a IEEE 21451 network for smart grid applications based on power line communications,” *IEEE Sensors J.*, vol. 15, no. 5, pp. 2460–2467, May 2015.
- [10] G. Artale *et al.*, “Smart interface devices for distributed generation in smart grids: The case of islanding,” *IEEE Sensors J.*, vol. 17, no. 23, pp. 7803–7811, Dec. 2017.
- [11] S. Rinaldi *et al.*, “Characterization of IP-based communication for smart grid using software-defined networking,” *IEEE Trans. Instrum. Meas.*, vol. 67, no. 10, pp. 2410–2419, Oct. 2018.
- [12] A. Sendin *et al.*, “Adaptation of powerline communications-based smart metering deployments to the requirements of smart grids,” *Energies*, vol. 8, no. 12, pp. 13481–13507, 2015.
- [13] Study Report III, *Electromagnetic Interference Between Electrical Equipment/Systems in the Frequency Range Below 150 kHz*, Standard SC205A/Sec0400/R, CENELEC, Oct. 2015.
- [14] G. Chu, J. Li, and W. Liu, “Narrow band power line channel characteristics for low voltage access network in China,” in *Proc. IEEE 17th Int. Symp. Power Line Commun. Appl.*, Mar. 2013, pp. 297–302.
- [15] C. M. De Dominicis, A. Flammini, S. Rinaldi, M. Rizzi, and A. Vezzoli, “Characterization of multi-standard power line communication on low-voltage grid,” in *Proc. IEEE Int. Instrum. Meas. Technol. Conf. (I2MTC)*, May 2013, pp. 31–36, doi: [10.1109/I2MTC.2013.6555375](https://doi.org/10.1109/I2MTC.2013.6555375).
- [16] F. Passerini and A. M. Tonello, “Smart grid monitoring using power line modems: Anomaly detection and localization,” *IEEE Trans. Smart Grid*, vol. 10, no. 6, pp. 6178–6186, Nov. 2019.
- [17] F. Passerini and A. M. Tonello, “Power line fault detection and localization using high frequency impedance measurement,” in *Proc. IEEE Int. Symp. Power Line Commun. Appl. (ISPLC)*, 2017, pp. 1–5.
- [18] Y. Huo, G. Prasad, L. Atanackovic, L. Lampe, and V. C. M. Leung, “Grid surveillance and diagnostics using power line communications,” in *Proc. IEEE Int. Symp. Power Line Commun. Appl. (ISPLC)*, Apr. 2018, pp. 1–6.

- [19] D. Liang, S. Ge, H. Guo, Y. Wang, Z. Liang, and C. Chen, "Monitoring power line faults using impedance estimation algorithms in power line communication equipment," in *Proc. 10th Int. Conf. Power Energy Syst. (ICPES)*, Dec. 2020, pp. 404–408.
- [20] D. Liang, H. Guo, and T. Zheng, "Real-time impedance estimation for power line communication," *IEEE Access*, vol. 7, pp. 88107–88115, 2019.
- [21] D. Liang, H. Guo, and T. Zheng, "Impedance tracking and estimation using power line communications," in *Proc. IEEE Int. Symp. Power Line Commun. Appl. (ISPLC)*, Apr. 2019, pp. 1–6.
- [22] L. Capponi, I. Fernandez, D. Roggo, A. Arrinda, I. Angulo, and D. De La Vega, "Comparison of measurement methods of grid impedance for narrow band-PLC up to 500 kHz," in *Proc. IEEE 9th Int. Workshop Appl. Meas. Power Syst. (AMPS)*, Sep. 2018, pp. 1–6.
- [23] I. Fernández, A. Arrinda, I. Angulo, D. D. L. Vega, N. Uribe-Pérez, and A. Llano, "Field trials for the empirical characterization of the low voltage grid access impedance from 35 kHz to 500 kHz," *IEEE Access*, vol. 7, pp. 85786–85795, 2019.
- [24] G. Hallak, C. Nieß, and G. Bumiller, "Accurate low access impedance measurements with separated load impedance measurements on the power-line network," *IEEE Trans. Instrum. Meas.*, vol. 67, no. 10, pp. 2282–2293, Oct. 2018, doi: [10.1109/TIM.2018.2814138](https://doi.org/10.1109/TIM.2018.2814138).
- [25] C. Nieß, J.-P. Kitzig, and G. Bumiller, "Measurement system for time variable subcycle impedance on power lines," in *Proc. IEEE Int. Instrum. Meas. Technol. Conf. (I2MTC)*, May 2021, pp. 1–6, doi: [10.1109/I2MTC50364.2021.9459875](https://doi.org/10.1109/I2MTC50364.2021.9459875).
- [26] P. S. Sausen, A. Sausen, M. De Campos, L. F. Sauthier, A. C. Oliveira, and R. R. Emmel Junior, "Power line communication applied in a typical Brazilian urban power network," *IEEE Access*, vol. 9, pp. 72844–72856, 2021.
- [27] F. Passerini and A. M. Tonello, "Analysis of high-frequency impedance measurement techniques for power line network sensing," *IEEE Sensors J.*, vol. 17, no. 23, pp. 7630–7640, Dec. 2017.
- [28] G. Artale *et al.*, "Implementation of a PLC field analyzer on a G3 modem platform," in *Proc. IEEE Int. Instrum. Meas. Technol. Conf. (I2MTC)*, May 2021, pp. 1–3.
- [29] *Narrowband Orthogonal Frequency Division Multiplexing Power Line Communication Transceivers—Power Spectral Density Specification*, Recommendation, document ITU-T G 9901.
- [30] *Narrowband Orthogonal Frequency Division Multiplexing Power Line Communication Transceivers for G3-PLC Networks*, Recommendation, document ITU-T G 9903, Aug. 2017.
- [31] G. Artale *et al.*, "PQ and harmonic assessment issues on low-cost smart metering platforms: A case study," *Sensors*, vol. 20, no. 21, p. 6361, Nov. 2020.
- [32] *E5080A ENA Vector Network Analyzer, Data Sheet 5992-0291EN*, Keysight Technologies, Santa Rosa, CA, USA. Accessed: Jun. 26, 2020. [Online]. Available: <https://www.keysight.com/it/en/assets/7018-04644/data-sheets/5992-0291.pdf>
- [33] *Keysight 85032F Type-N 50 Calibration Kit, User's and Service Guide*, Keysight Technologies, Santa Rosa, CA, USA. Accessed: Feb. 3, 2022. [Online]. Available: <https://www.keysight.com/it/en/assets/9018-01295/user-manuals/9018-01295.pdf>

Giovanni Artale (Member, IEEE) received the M.S. degree in electronic engineering and the Ph.D. degree in electronic and telecommunication engineering from the University of Palermo, Palermo, Italy, in 2010 and 2014, respectively.

He is currently a Researcher with the Department of Engineering, University of Palermo. His current research interests include low-frequency harmonic analysis algorithms, power line communications, and smart grids.

Giuseppe Caravello received the M.S. degree in electrical engineering from the University of Palermo, Palermo, Italy, in 2018, where he is currently pursuing the Ph.D. degree in energy and Information and Communication Technology (ICT).

His research interests include power system measurement and monitoring, impacts of distributed generations on power systems, artificial intelligence, and energy storage systems.

Antonio Cataliotti (Member, IEEE) received the M.S. and Ph.D. degrees in electrical engineering from the University of Palermo, Palermo, Italy, in 1992 and 1998, respectively.

He is currently a Full Professor of electrical and electronic measurements with the Department of Engineering, University of Palermo. His current research interests include power quality measurements, power line communications, and smart grids.

Valentina Cosentino (Member, IEEE) received the M.S. and Ph.D. degrees in electrical engineering from the University of Palermo, Palermo, Italy, in 2001 and 2005, respectively.

She is currently an Associate Professor of electrical and electronic measurements with the Department of Engineering, University of Palermo. Her current research interests include energy and power quality measurements, detection of disturbances sources in power systems, virtual instrumentation, and smart grids.

Dario Di Cara (Member, IEEE) received the M.S. and Ph.D. degrees in electrical engineering from the University of Palermo, Palermo, Italy, in 2005 and 2009, respectively.

Since 2012, he has been a Researcher with National Research Council, Palermo. His current research interests include power quality measurements, current transducers characterization in nonsinusoidal conditions, power line communications, and smart grids.

Riccardo Fiorelli received the bachelor's degree in electronics engineering from the Politecnico di Milano, Milan, Italy, in 2003.

In 2003, he joined STMicroelectronics, Agrate Brianza, Italy. Since 2005, he has been a senior application engineer for industrial products. He is especially an expert in the power line communication systems and application fields.

Salvatore Guaiana received the M.S. degree in electronics and photonics engineering and the Ph.D. degree in energy and information technologies from the University of Palermo, Palermo, Italy, in 2012 and 2019, respectively.

He is currently a Research Fellow with the Institute of Marine Engineering, National Research Council, Palermo. His current research interests include power line communications, the development of microcontroller systems, and communications protocols for smart grids applications.

Nicola Panzavecchia received the M.S. degree in computer science and the master's degree in domotics and building automation from the University of Palermo, Palermo, Italy, in 2007 and 2011, respectively.

Since 2007, he has been a consultant, a programmer, and a web system administrator. He is currently a Researcher with the National Research Council, Palermo. His current research interests include software development for energy management and embedded systems, smart grids, and power line communications.

Giovanni Tinè (Member, IEEE) received the M.S. degree in electronic engineering and the Ph.D. degree in electronics, computer science, and telecommunications engineering from the University of Palermo, Palermo, Italy, in 1990 and 1994, respectively.

Since 2000, he has been a Researcher with the National Research Council, Palermo. His main scientific interests are distributed measurement system for smart grids, power-line communication in medium- and low-voltage systems, electromagnetic compatibility (EMC), and intelligent electronic devices for smart grids.